EUROFUSION WP15ER-PR(15) 14360

I Jonane et al.

Temperature-dependent EXAFS study of the local structure and lattice dynamics in cubic Y2O3

Preprint of Paper to be submitted for publication in
Journal of Physics: Condensed Matter

This work has been carried out within the framework of the EUROfusion Consortium and has received funding from the Euratom research and training programme 2014-2018 under grant agreement No 633053. The views and opinions expressed herein do not necessarily reflect those of the European Commission.

Temperature-dependent EXAFS study of the local structure and lattice dynamics in cubic Y_2O_3

I. Jonane[1], K. Lazdins[1], J. Timoshenko[1], A. Kuzmin[1], J. Purans[1], P. Vladimirov[2], T. Gräning[2], J. Hoffmann[2]

[1] Institute of Solid State Physics, University of Latvia, Kengaraga street 8, LV-1063 Riga, Latvia

[2] Institute for Applied Materials-Applied Materials Physics, Karlsruhe Institute of Technology, Eggenstein-Leopoldshafen, PO Box 3640, 76021 Karlsruhe, Germany

E-mail: janis.timoshenko@gmail.com

E-mail: a.kuzmin@cfi.lu.lv

Abstract. The local structure and lattice dynamics in cubic Y_2O_3 were studied at the Y K-edge by X-ray absorption spectroscopy in the temperature range from 300 to 1273 K. The temperature dependence of the extended X-ray absorption fine structure was successfully interpreted using classical molecular dynamics (MD) and a novel reverse Monte Carlo method, coupled with evolutionary algorithm. The obtained results allowed us to follow temperature dependence of the yttria atomic structure up to ∼6 Å and to validate two force-field models.

Submitted to: *J. Phys.: Condens. Matter*

1. Introduction

Yttrium sesquioxide (Y_2O_3) is an important technological material which is employed in pure, doped or nanosized forms. For instance, it is used as a phosphor in optical display and lighting applications [1, 2, 3], in rare-earth ion doped lasers [4, 5], for ethanol steam reforming in fuel-cell applications [6] and in a production of ceramic materials [7]. During the last decade Y_2O_3 attracted much attention since it was shown that mechanical properties and radiation resistance of steels can be improved by an addition of yttrium compounds during the manufacturing process leading to a formation of nanosized yttria within the steel matrix [8, 9, 10]. Such oxide dispersion strengthened (ODS) steels are considered now as a promising structural materials for concentrated solar power plants and jet engines, and, in particular, for fusion and fission nuclear reactors [11].

The understanding and improving of ODS steel properties at the atomic scale represents a complicated task whose solution requires the use of modern experimental and theoretical approaches. Among different experimental techniques X-ray absorption spectroscopy (XAS) is able to probe the local atomic structure and lattice dynamics in bulk and nanocrystalline materials around both concentrated and diluted elements [12, 13, 14]. Therefore its application to the case of ODS steels was naturally started during the last ten years [15, 16, 17, 18, 19, 20, 21]. On the other hand, one expects that large-scale molecular dynamics (MD) [22, 23] and Monte Carlo [24, 25] simulations will contribute to the interpretation and prediction of experimental results. The reliability of these theoretical models is directly related to how well the interatomic interactions can be described in the steel matrix, within the oxide nanoparticles and between the nanoparticles and the matrix. This question can be addressed using recently developed method [26], which allows validation of interatomic potentials by direct comparison of experimentally measured extended X-ray absorption fine structure (EXAFS) with theoretically simulated one. However, the accurate simulation of yttrium oxide nanoparticles, embedded in steel matrix, or even of freestanding yttria particles is truly challenging, therefore we have started from their bulk ancestor.

Cubic yttrium sesquioxide (c-Y_2O_3), known also as α-Y_2O_3, has complex crystallographic structure and belongs to the space group $Ia\bar{3}$ with $Z = 16$ (Fig. 1). Its lattice parameter is equal to $a_0 = 10.604$ Å at $T = 300$ K [27] (the range of values, reported in the literature, is 10.6021–10.6042 Å [28]). There are two non-equivalent yttrium atoms Y1 and Y2 located at the Wyckoff positions 8b(0.25, 0.25, 0.25) and 24d(u, 0, 0.25) ($u = -0.0326$ at $T = 300$ K [27]), respectively, and the oxygen atoms occupy 48c(x, y, z) positions ($x = 0.3911$, $y = 0.1519$, $z = 0.3806$ at $T = 300$ K [27]). The structural parameters do not change significantly below the room temperature down to 77 K [29]. However, the lattice parameter of c-Y_2O_3 increases nonlinearly up to 2512±25 K, where a phase transition into the fluorite-type structure (space group $Fm\bar{3}$) occurs, followed by melting at 2705±25 K [30].

The lattice dynamics of c-Y_2O_3 was studied experimentally and theoretically. In [31] neutron inelastic scattering measurements of the phonon density of states and

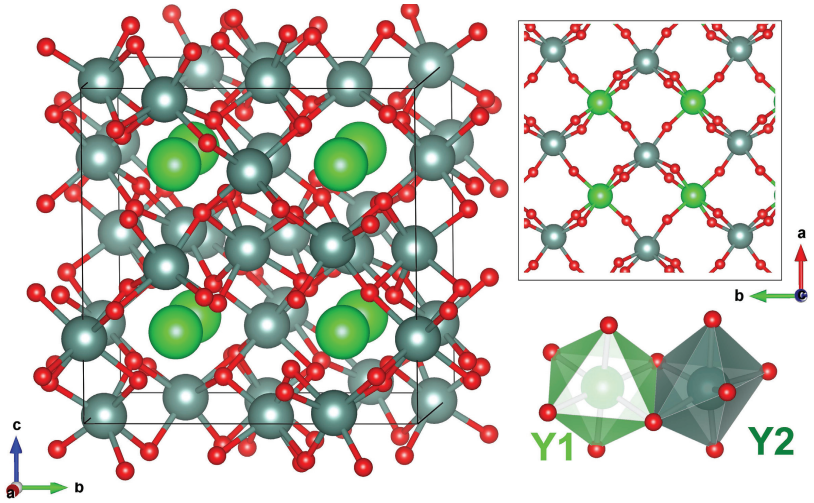

Figure 1. (Color online) Crystal structure of cubic Y_2O_3 [27, 29]. The regular and distorted octahedra around non-equivalent yttrium atoms (Y1 and Y2) are also shown.

lattice dynamic calculations using first-principles density functional theory and force-field interatomic potential model were performed.

Classical molecular dynamics (MD) simulation of c-Y_2O_3 were reported in several papers [31, 32, 33, 34], and the results, obtained in the recent two [31, 34], will be considered further.

In this study we have employed two advanced methods: (i) MD-EXAFS [26] and (ii) the novel reverse Monte Carlo/evolutionary algorithm approach (RMC/EA-EXAFS) [35] for the interpretation of temperature dependent Y K-edge EXAFS in c-Y_2O_3. MD-EXAFS method [26] allowed us to validate the quality of the most recent force-field models based on pair potentials [31, 34]. The obtained results are compared with those determined by the RMC/EA-EXAFS method [35, 36], which provides better description of the distorted local environment around yttrium atoms.

These two methods have been successfully employed by us recently to a number of crystalline materials as $SrTiO_3$ [26], ReO_3 [35, 36, 37, 38], $LaCoO_3$ [39], Ge [36, 40], NiO [41], H_xReO_3 [35], ZnO [42, 43] and various tungstates [44, 45, 46].

2. Experimental and data analysis

X-ray absorption spectra of cubic Y_2O_3 (99.99%, Sigma-Aldrich) were recorded at the Y K-edge (17038 eV) in transmission mode at the ELETTRA (Trieste, Italy) XAFS bending-magnet beamline [47]. The storage ring operated in the top-up multibunch mode at the energy $E = 2$ GeV and current $I = 310$ mA. The synchrotron radiation was monochromatized using a Si(111) double-crystal monochromator, and its intensity before and after the sample was measured by two ionization chambers. Yttrium metallic foil (99%, GoodFellow) was used for energy calibration. Polycrystalline c-Y_2O_3 powder was mixed with boron nitride and pressed into pellets. The sample thickness was

optimized to obtain the absorption Y K-edge jump value $\Delta\mu \approx 1$. The sample temperature was controlled using the l'Aquila-Camerino glass furnace [47] for high temperature measurements in the range from 20 to 1000°C.

The experimental Y K-edge EXAFS spectra were extracted using the conventional procedure [13, 48] and are shown together with their Fourier transforms (FT's) in Fig. 2. The position of the photoelectron energy origin E_0 was set at the 17050 eV to be in agreement with the theoretical one obtained by the FEFF8 code [49]. The first peak in FT at ∼1.7 Å is due to the contribution of the first coordination shell (six closest oxygen atoms) around the absorbing yttrium atom, whereas the second peak at 3.5 Å, having a double-peak shape at room temperature, originates mainly due to the second and third coordination shells formed by yttrium atoms. Note that six Y atoms in the second coordination shell are located at about 3.5 Å from the absorbing yttrium atom, and their YO_6 octahedra share the common edge with that of the absorbing yttrium; the distance between six Y atoms in the third coordination shell and the absorbing yttrium atom is about 4.0 Å, and their YO_6 octahedra are connected through a common vertex (Fig. 1).

3. Molecular dynamics simulations

Classical molecular dynamics (MD) simulations were performed using the GULP code [50, 51] in the canonical (NVT) ensemble with periodic boundary conditions. The simulation box had a size of the $2a_0 \times 2a_0 \times 2a_0$ supercell including 640 atoms. The starting configuration was set to the mean crystallographic c-Y_2O_3 structure [27]. Nosé-Hoover thermostat [52] was used to keep the required average temperature during each simulation. The Newton's equations of motion were integrated using the Verlet leapfrog algorithm [53] with a time step of 0.5 fs. The equilibration and production times were 20 ps each. The simulations were performed at the temperatures in the range from 24 to 1000°C, corresponding to that of the EXAFS experiments. A set of 4000 atomic configurations were accumulated during each production run, and the Y K-edge EXAFS spectra were calculated for two non-equivalent yttrium atoms (Y1 and Y2) in each MD configuration using ab initio real-space multiple-scattering FEFF8 code [49, 54]. Finally, the configuration-averaged Y K-edge EXAFS spectra were obtained [26] and used for the direct comparison with the experimental ones.

The multiple-scattering contributions were accounted up to the 7th order. Note, however, that the influence of such contributions for investigated material is quite small. The calculation of the cluster potential was performed only once for the mean crystallographic c-Y_2O_3 structure [27], thus neglecting its small variation due to thermal disorder. The complex exchange-correlation Hedin–Lundqvist potential and default values of muffin-tin radii ($R_{\rm mt}$(Y)=1.57 Å and $R_{\rm mt}$(O)=1.06 Å), as provided within the FEFF8 code [49], were employed.

Two force-field models [31, 34], based on the rigid-ion Buckingham potential, were

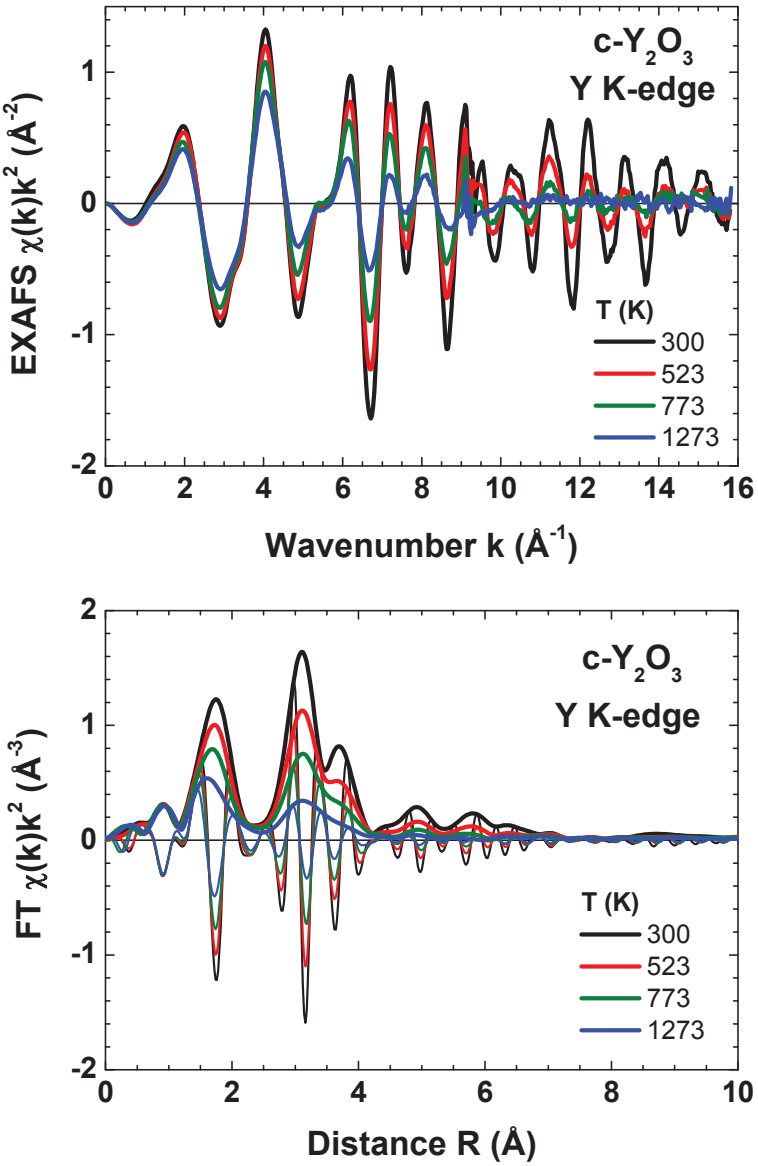

Figure 2. (Color online) Temperature dependence of the experimental Y K-edge EXAFS spectra $\chi(k)k^2$ and their (phase-uncorrected) Fourier transforms (FT's) for c-Y_2O_3 at several selected temperatures. Both the magnitude and imaginary parts of the FTs are shown.

used in MD simulations to describe interactions in c-Y_2O_3 (Table 1)

$$U_{ij}(r_{ij}) = A_{ij}\exp(-\frac{r_{ij}}{\rho_{ij}}) - \frac{C_{ij}}{r_{ij}^6} + \frac{q_i q_j e^2}{r_{ij}}. \quad (1)$$

The Coulomb interactions were described using the effective ion charges q(Y)=+2.4 and q(O)=−1.6 in the first model (Model1) [31], whereas the formal ion charges were assumed q(Y)=+3 and q(O)=−2 in the second model (Model2) [34].

Several properties of c-Y_2O_3 as the lattice parameter, bulk modulus (B_0) and elastic constants (C_{11}, C_{12} and C_{44}) were calculated using two force-field models [31, 34] and

Table 1. Buckingham potential parameters for the Y–O and O–O atom pairs used in molecular dynamics simulations.

Pair of atoms	A (eV)	ρ (Å)	C (eVÅ^6)
	Model1 [31]		
Y–O	1822	0.309042	0.0
O–O	1822	0.305726	100.0
	Model2 [34]		
Y–O	1642.724	0.353197	104.180
O–O	2056.49	0.361402	271.761

Table 2. Experimental [29, 55] and calculated properties of c-Y_2O_3.

	Experiment	Model1 [31]	Model2 [34]
Lattice parameter (Å)	10.6073	10.58	10.61
Bulk modulus B_0 (GPa)	156	137	182
Elastic constant C_{11} (GPa)	223.7	204	292
Elastic constant C_{12} (GPa)	112.4	103	127
Elastic constant C_{44} (GPa)	74.6	79	85

are compared with the available experimental data [29, 55] in Table 2. As one can see, both models reproduce the experimental values equally well.

The experimental Y K-edge EXAFS and configuration-averaged MD-EXAFS spectra, calculated using two models, and their Fourier transforms are compared in Fig. 3 for the two utmost temperatures (300 and 1273 K). The first model (Model1) gives overall good agreement with experimental data, except for some small discrepancy in the FT peaks amplitude at 300 K due to the underestimation of the YO_6 octahedra distortion in the model. The second model (Model2) fails significantly at 300 K in the description of peaks located between 1 and 4 Å in FT, and the discrepancy remains for the first shell at 1273 K. In fact, the difference at 300 K for the Model2 is also well observed in k-space.

4. Reverse Monte Carlo simulations

Reverse Monte Carlo (RMC) method [56, 36] allows one to construct a structure model of the material based on the available experimental data (EXAFS in our case) only and does not require the knowledge of interatomic potentials, which is a crucial point in MD simulations. Additionally the RMC method can be applied to study the materials also at cryogenic temperatures, where the MD approach fails due to the neglect of quantum effects. On the other hand, the extraction of dynamical information

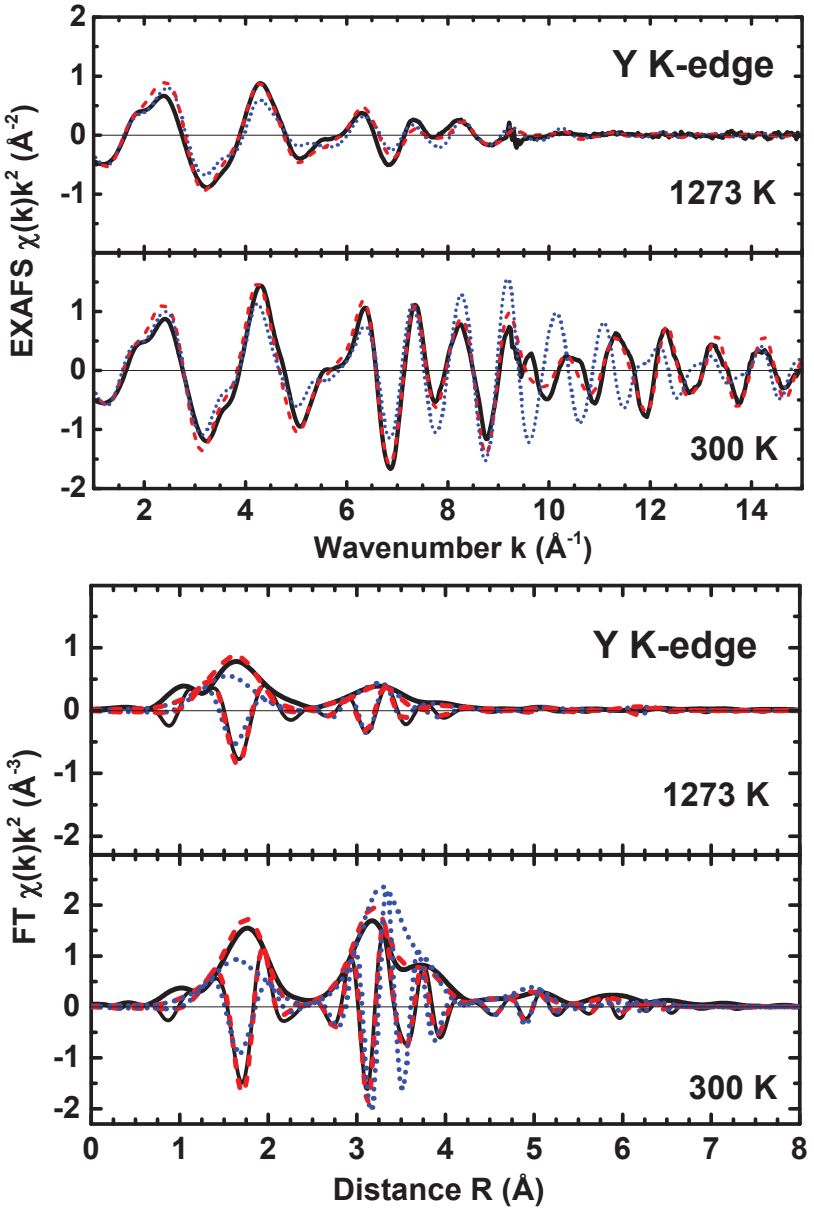

Figure 3. (Color online) Comparison of the experimental (solid lines) and calculated by MD-EXAFS method (dashed lines – Model1 [31] and dotted lines – Model2 [34]) Y K-edge EXAFS spectra $\chi(k)k^2$ and their (phase-uncorrected) Fourier transforms for c-Y_2O_3 at 300 and 1273 K. Both the magnitude and imaginary parts of the FTs are shown.

(interatomic forces, frequencies of atomic oscillations) from the results of RMC process is not straightforward. Therefore both approaches, MD and RMC, complement each other.

Recently we have proposed an enhanced RMC approach for the analysis of EXAFS data from crystalline materials, based on the use of evolutionary algorithm (EA). The combined RMC/EA scheme allows us to perform accurate analysis of EXAFS data from distant coordination shells, taking into account static and thermal disorder as well

as multiple scattering effects, and can be applied even for complex materials with low symmetry [35, 45]. As in the conventional reverse Monte Carlo method, the 3D structure model of a material is optimized in the RMC/EA scheme via the consequent proposal of random changes of atomic coordinates, and the agreement between the experimental and configuration-averaged EXAFS spectra, calculated for the proposed structure model, is used as the only criterium for the acceptance or rejection of proposed move. This configuration-averaged EXAFS spectrum is obtained from ab initio multiple-scattering calculations performed by the FEFF8 code [49]. Implementation of the evolutionary algorithm in the conventional RMC scheme significantly improves the convergence of the simulations: in this case we use not just one, but several (32 in this study) structure models of the material simultaneously. The information exchange between the simulated structure models allows us to find the solution – the average atomic configuration that gives the best possible description of experimental data – much faster [35].

As in MD simulations, the model of crystalline yttria in RMC/EA-EXAFS analysis is constructed as an infinite crystal employing periodic boundary conditions for the supercell composed of $2a_0 \times 2a_0 \times 2a_0$ unit cells of cubic Y_2O_3. The value of the lattice parameter a_0=10.607 Å was fixed at the experimental value for crystalline yttria obtained from neutron powder diffraction experiment [29]. The Y K-edge EXAFS spectra were calculated for both non-equivalent yttrium positions (Y1 and Y2) separately, and then added together with weights of 1/4 and 3/4, which correspond to the ratio of Y1 and Y2 atoms in cubic Y_2O_3 structure, to obtain the total configuration-averaged EXAFS spectrum. The latter was used for the comparison with the experimental EXAFS data. The EXAFS calculations were performed using the same scattering paths and cluster potential as for the MD simulations. The experimental and calculated Y K-edge EXAFS spectra at each iteration were compared using Morlet wavelet transform (WT) [57, 58, 59] in the k-space range from 3.5 to 14.5 Å^{-1} and in the R-space range from 1.0 to 6.9 Å. This allowed us to account for the features of EXAFS spectra in k and R spaces simultaneously.

At each temperature a good agreement between the experimental and calculated Y K-edge EXAFS spectra (Figs. 4 and 5) was achieved after several thousands of RMC/EA iterations. As one can see, RMC/EA modelling, unlike MD approach, allowed us to obtain a very good description of all features of EXAFS in k and R spaces at all temperatures. The final atomic configurations then were used to estimate the structure parameters of interest. The final set of atomic coordinates was also used to evaluate the importance of a contribution from the multiple-scattering (MS) effects to the total EXAFS spectrum (Fig. 4). As one can see, the MS contribution in cubic Y_2O_3 is quite small but not negligible in all k-range. Moreover, an account for the MS effects is important to correctly describe the FT peaks at ∼3.7 Å and 6 Å: here the main MS contributions come from the octahedral environment around the absorbing yttrium atoms in the first (oxygen) and second (yttrium) coordination shells, respectively.

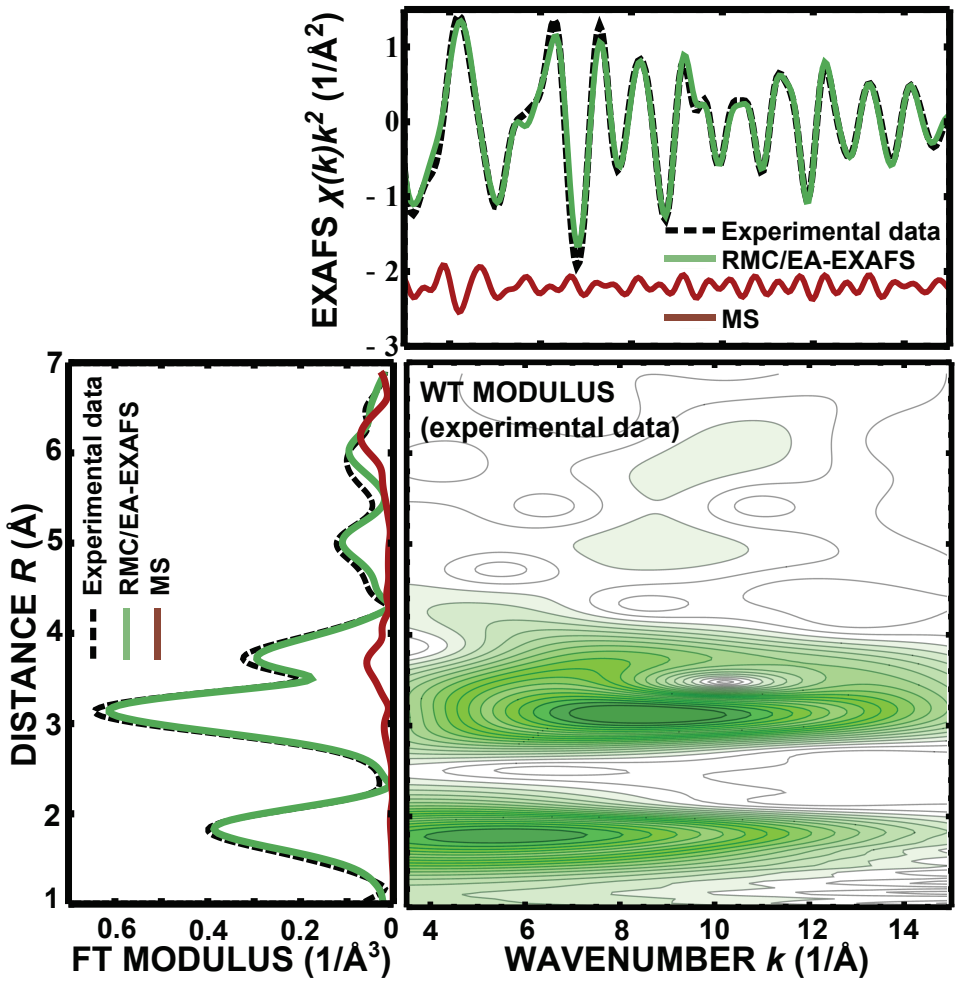

Figure 4. (Color online) Results of RMC/EA-EXAFS calculations for c-Y_2O_3 at room temperature: comparison of experimental and calculated (RMC/EA) Y K-edge EXAFS spectra $\chi(k)k^2$ (upper panel) and their Fourier transforms (bottom left panel), and the Morlet wavelet image of the experimental Y K-edge EXAFS spectrum (bottom right panel). Multiple-scattering (MS) contribution to the total EXAFS spectrum is also shown.

5. Discussion

To compare the structure models, obtained by MD and RMC/EA simulations, one can calculate the atomic radial distribution functions (RDFs) around both Y1 and Y2 (Fig. 6). Note that while the distribution of atoms in outer coordination shells of Y1 and Y2 differs significantly, the first three peaks of RDFs have close shapes and positions for both non-equivalent yttrium sites. We will limit our further discussion to these peaks only.

Comparison of RDFs for Y–O and Y–Y atom pairs at room temperature indicates that both RMC/EA and MD methods give close results. However, one can note that the width of peaks in RDF around Y1 is systematically narrower and, hence, the peaks are higher in the case of MD results.

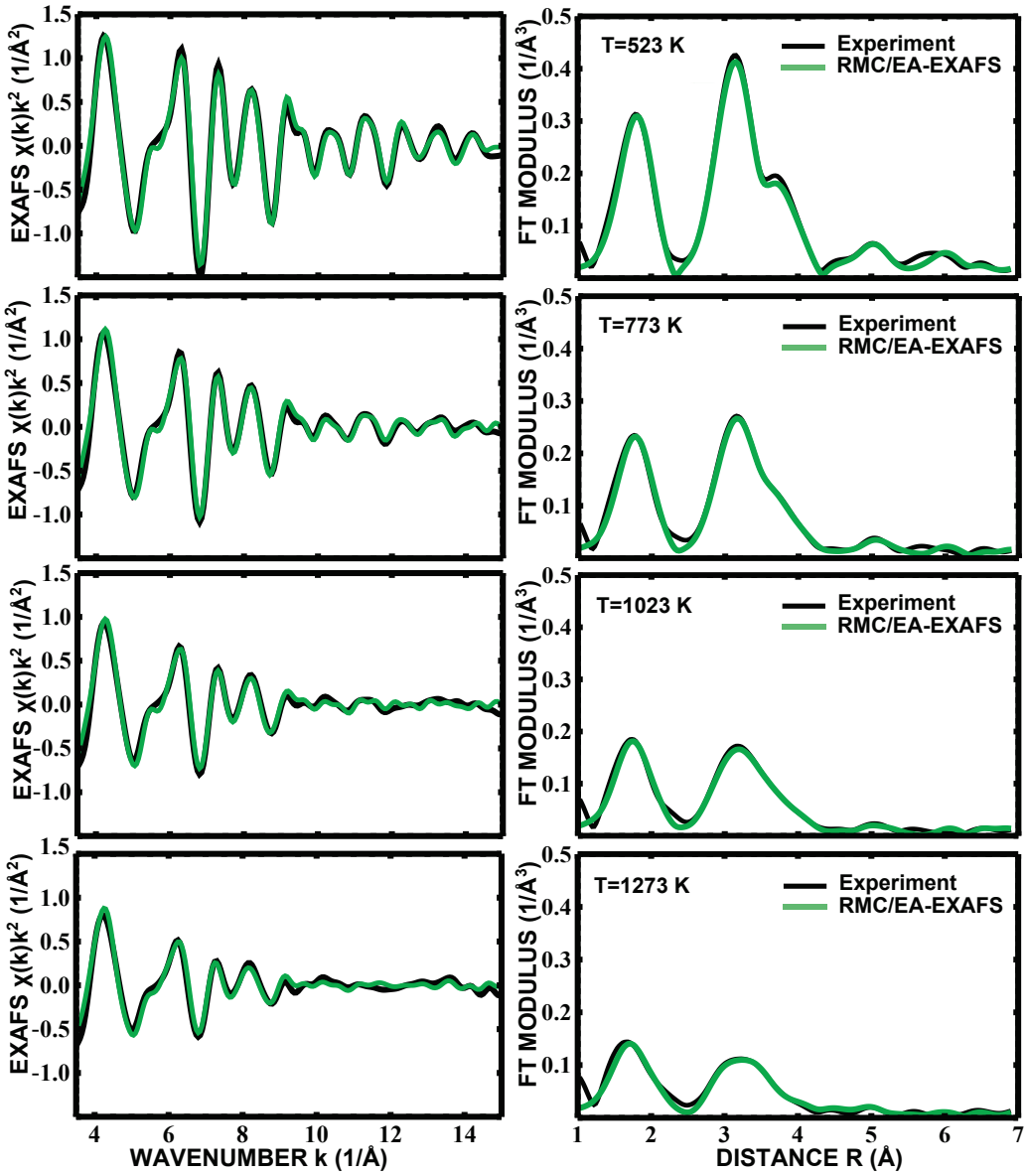

Figure 5. (Color online) Results of RMC/EA-EXAFS calculations for c-Y_2O_3 at temperatures from 523 up to 1273 K: comparison of the experimental and calculated (RMC/EA) Y K-edge EXAFS spectra $\chi(k)k^2$ (left panels) and their Fourier transforms (right panels).

To make comparison more quantitative and to follow temperature dependent variations, we have extracted the mean square relative displacement (MSRD) factors, containing contributions both from static and thermal disorder, from the widths of RDF peaks: their temperature dependencies for the first three coordination shells are shown in Fig. 7. The uncertainties of RMC/EA results were estimated from the results of calculations repeated several times with different sequences of pseudo-random numbers [35]. One can see that MSRD factors, obtained by MD and RMC/EA methods, are

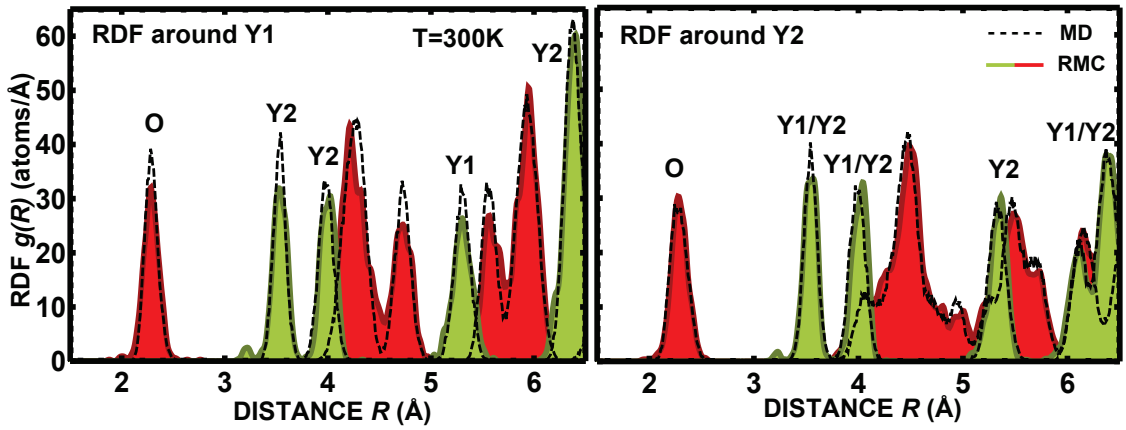

Figure 6. (Color online) RDFs around non-equivalent Y1 and Y2 sites, obtained in RMC/EA and MD (Model1) simulations for $T = 300$ K.

close at room temperature, and the temperature dependencies of MSRD factors for all three coordination shells of yttrium are also close.

Our RMC/EA results for the first coordination shell (Y–O pair, Fig. 7(b)) suggest that all four non-equivalent Y–O bonds (one Y1–O and three Y2–O) have close MSRD values and cannot be discriminated within uncertainties. Temperature-dependencies of the obtained MSRDs were best fitted using correlated Einstein model [60] (solid line in Fig. 7(b)). Using the obtained value of the Einstein frequency ω_E, one can estimate the effective bond-strength constant $\kappa = \omega_E^2 \mu$, where μ is reduced mass of the atomic pair. Its value for Y–O bond $\kappa = (89 \pm 4)$ N/m is close to that determined by infra-red and Raman spectroscopies (103 N/m in [61] and 108 N/m in [62]). As was mentioned before, when one compares the MSRD values, obtained in the RMC/EA simulations, with the MD results, one can see, they are in a reasonable agreement. Thus one can conclude that the pairwise Y–O interactions are described with sufficient accuracy in the used force field model (Model1).

Similar conclusions can be drawn for the second and third coordination shells (Y–Y pairs), Fig. 7(c) and 7(d): RMC/EA and MD give close MSRD values. Some small differences in MSRD factors for Y1–Y2 and Y2–Y2 pairs in the second coordination shell and Y1–Y2 pair in the third coordination shell can be, nevertheless, observed. Our results suggest that the static contribution to the MSRD for Y1–Y2 pair in the second coordination shell is slightly larger than that for corresponding Y2–Y2 pair. When best-fitted with the Einstein model [60], the obtained effective bond-strength constant $\kappa = (116 \pm 8)$ N/m is the same for both types of Y–Y pairs in the second coordination shell. In the third coordination shell the differences between MSRD values for Y1–Y2 and Y2–Y2 pairs cannot be detected within the precision of our method, but the corresponding effective bond-strength constant $\kappa = (107 \pm 9)$ N/m is slightly smaller than that for the second coordination shell.

The temperature dependencies of isotropic mean-square displacement (MSD)

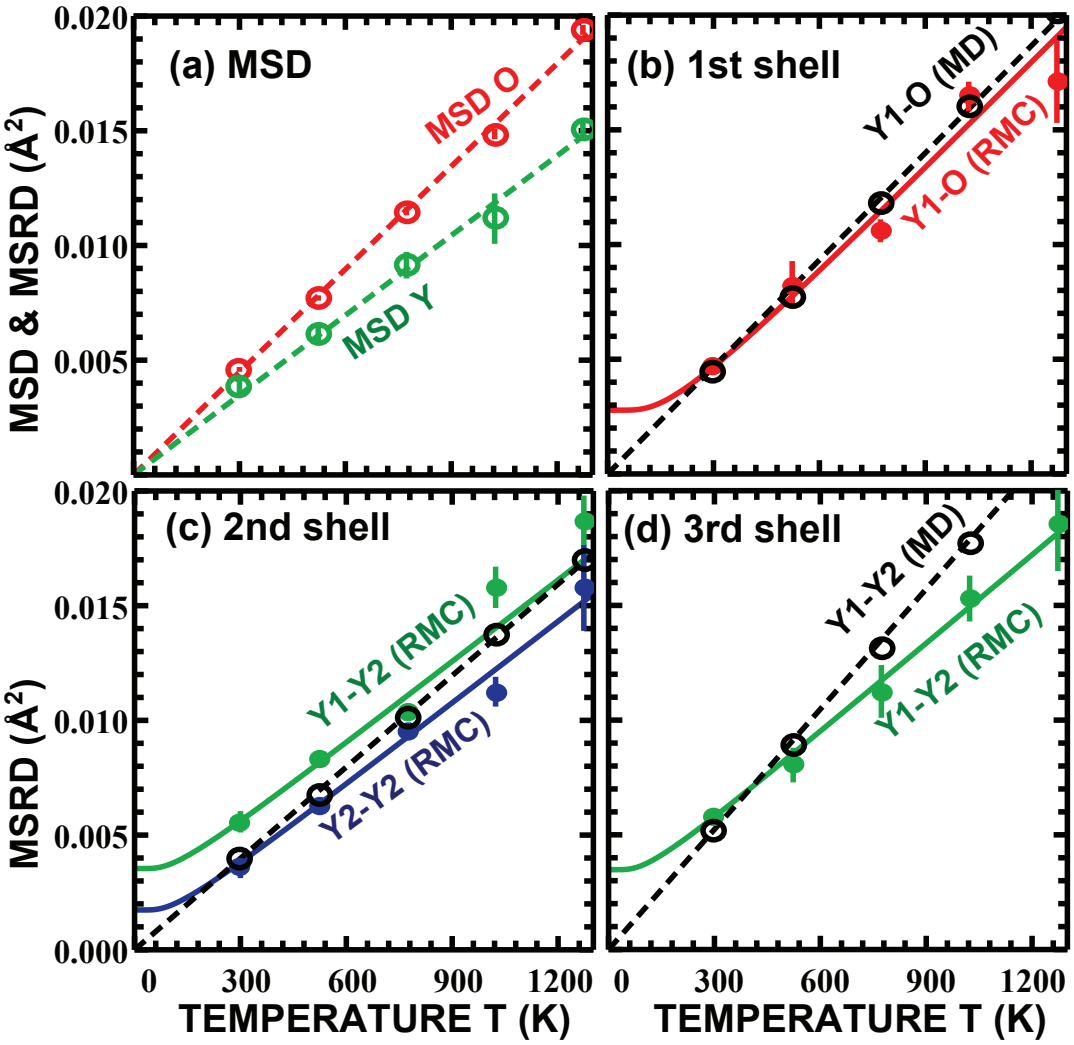

Figure 7. (Color online) Calculated MSD (a) and MSRD factors for the first (Y–O) coordination shell (b), for the second (Y–Y) coordination shell (c) and for the third (Y–Y) coordination shell (d). MSD factors are calculated from MD simulations for Model1. Dashed straight lines and open circles refer to MSRD and MSD values, obtained from MD simulations for Model1. MSRD values obtained by RMC/EA method are shown by filled circles, while the solid lines correspond to their fit by the Einstein model.

factors for Y and O atoms are shown in Fig. 7(a). These values were extracted from MD simulations only: as will be discussed below, for c-Y_2O_3 the analysis by RMC/EA-EXAFS method is not sensitive enough to obtain reliable MSD data.

The MSD and MSRD values for the i-j atom pair are related as $\mathrm{MSRD}_{ij} = \mathrm{MSD}_i + \mathrm{MSD}_j - 2\sqrt{\mathrm{MSD}_i}\sqrt{\mathrm{MSD}_j}\phi$, where ϕ is a dimensionless correlation parameter [63], which is equal to $+1$ for perfectly in-phase atom motion, to zero for completely independent motion, and to -1 for perfectly antiphase motion. For materials without phase transitions one can expect that the value of ϕ depends on temperature in the low-temperature region, but reaches some saturation value at high-temperatures. Using the results of our MD simulations for the Model1, we have found (Fig. 8) that the correlation

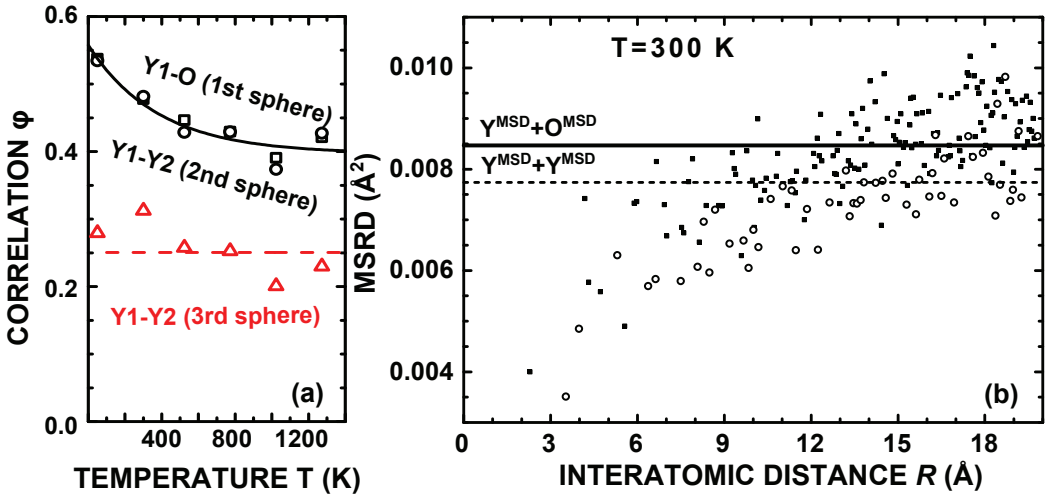

Figure 8. Panel (a): temperature dependence of the dimensionless correlation parameter ϕ for the nearest Y–O and Y–Y bonds; solid and dashed lines – guides for the eye. Panel (b): calculated MSRD factors for Y–O (open circles) and Y–Y (solid squares) plotted versus the interatomic distance R; solid line is a sum of MSDs for Y and O, dashed line is a sum of two MSDs of Y. All results are obtained from MD simulations at 300 K using the force-field model (Model1) from [31].

parameter is $\phi = 0.55$ at 50 K and decreases down to $\phi = 0.40$ at 1273 K for both first (Y1–O pairs) and second (Y1–Y2 pairs) coordination shells, indicating prevalent in-phase motion of nearest neighbours in c-Y_2O_3. In the third (Y1–Y2 pairs) coordination shell the correlation $\phi \approx 0.25$ is small and remains constant at all temperatures within the simulation error.

The variation of MSRDs for nearest Y–O and Y–Y as a function of the interatomic distance was calculated at $T = 300$ K from a set of atomic coordinates obtained by MD simulations for the Model1 and is shown in Fig. 8. The values of MSRDs increase and reach the sum of the MSDs values for distant shells at about 9–15 Å. Thus, the extraction of the MSD values from EXAFS data only (using, for instance, RMC/EA method) for crystalline yttria is, in principle, possible, but is challenging since it requires to have a high quality experimental data as well as to perform the analysis of distant coordination shells [64, 65]. The information on MSD factors is also encoded in the contribution of multiple-scattering effects, which can be analyzed using RMC/EA scheme [35]. Unfortunately, for investigated system the contribution of these effects is very small. At the same time, both MSD and MSRD values can be directly obtained from the MD simulations, validated in advance using EXAFS data.

6. Conclusions

Local atomic structure and lattice dynamics in cubic Y_2O_3 were studied in the temperature range from 300 to 1273 K by X-ray absorption spectroscopy. The experimental Y K-edge EXAFS data were analysed by reverse Monte Carlo/evolutionary

algorithm simulations and were also used to validate by the MD-EXAFS method [26] two force-field models [31, 34], which were employed in the classical molecular dynamics simulations and are based on the Born-Meyer-Buckingham potential. We have found that while both force-field models give close values of the lattice parameter, bulk modulus (B_0) and elastic constants (C_{11}, C_{12} and C_{44}) (Table 2) in rather good agreement with the available experimental data [29, 55], the second force-field model (Model2) from [34] fails to reproduce temperature dependence of the EXAFS spectra. Thus the EXAFS spectra provide additional information on the structure and dynamics of bulk cubic Y_2O_3, which allows one to discriminate such close theoretical models as in [31, 34].

The MD simulations performed using the force-field model (Model1) from [31] give configuration-averaged EXAFS spectra in a rather good agreement with the experimental data at all temperatures, except for small discrepancy in the broadening of the first and second coordination shells at 300 K. This discrepancy is due to the pair-potential model, which is not able to account properly for YO_6 octahedra distortions in cubic Y_2O_3. The results of the MD simulations also suggest a decrease of the correlation in atomic motion for nearest atom pairs in the first and second coordination shells with increasing temperature. At the same time, the correlation effects are smaller and remains constant for outer coordination shells.

RMC/EA approach allowed us to obtain more accurate structure model of cubic Y_2O_3 and to follow its evolution upon temperature increase. We have found that the difference in the dynamics of local surrounding around non-equivalent Y1 and Y2 sites is not large. At the same time, our analysis suggests that there are significant differences in the temperature effect on the interaction of Y–Y pairs in the second and third coordination shells, despite the fact that corresponding interatomic distances are close.

Temperature dependencies of MSRD factors, obtained in RMC/EA simulations, are close to those, obtained in MD simulations, thus one can conclude that the pairwise Y–O and Y–Y interactions are accounted rather well in the force-field model (Model1) developed in [31].

Acknowledgments

This work has been carried out within the framework of the EUROfusion consortium and has received funding from the Euratom research and training programme 2014-2018 under grant agreement No 633053. The views and opinions expressed herein do not necessarily reflect those of the European Commission. We gratefully acknowledge the assistance of the XAFS beamline staff members during the EXAFS experiment. The research leading to these results has received funding from the European Communitys Seventh Framework Programme (FP7/2007-2013) under Grant agreement No 312284.

References

[1] Igarashi T, Ihara M, Kusunoki T, Ohno K, Isobe T and Senna M 2000 *Appl. Phys. Lett.* **76** 1549
[2] Schmechel R, Kennedy M, von Seggern H, Winkler H, Kolbe M, Fischer R A, Xaomao L, Benker A, Winterer M and Hahn H 2001 *J. Appl. Phys.* **89** 1679
[3] Capobianco J A, Vetrone F, Boyer J C, Speghini A and Bettinelli M 2002 *J. Phys. Chem. B* **106** 1181
[4] Xu Y N, Gu Z Q and Ching W Y 1997 *Phys. Rev. B* **56** 14993
[5] Lu J, Lu J, Murai T, Takaichi K, Uematsu T, Ueda K, Yagi H, Yanagitani T and Kaminskii A A 2001 *Jap. J. Appl. Phys.* **40** L1277
[6] Sun J, Qiu X P, Wu F and Zhu W T 2005 *Int. J. Hydrogen Energ.* **30** 437
[7] Wang S, Zhang J, Luo D, Gu F, Tang D, Dong Z, Tan G, Que W, Zhang T, Li S and Kong L 2013 *Prog. Solid State Chem.* **41** 20
[8] Ukai S and Fujiwara M 2002 *J. Nucl. Mater.* **307-311** 749
[9] Klueh R, Maziasz P, Kim I, Heatherly L, Hoelzer D, Hashimoto N, Kenik E and Miyahara K 2002 *J. Nucl. Mater.* **307-311** 773
[10] Schneibel J, Liu C, Hoelzer D, Mills M, Sarosi P, Hayashi T, Wendt U and Heyse H 2007 *Scripta Mater.* **57** 1040
[11] Lindau R, Möslang A, Schirra M, Schlossmacher P and Klimenkov M 2002 *J. Nucl. Mater.* **307** 769
[12] Lee P A, Citrin P H, Eisenberger P and Kincaid B M 1981 *Rev. Mod. Phys.* **53** 769
[13] Aksenov V, Kovalchuk M, Kuzmin A, Purans Y and Tyutyunnikov S 2006 *Crystallogr. Rep.* **51** 908
[14] Yano J and Yachandra V 2009 *Photosynth. Res.* **102** 241
[15] Degueldre C, Conradson S and Hoffelner W 2005 *Comp. Mater. Sci.* **33** 3
[16] Pouchon M, Kropf A, Froideval A, Degueldre C and Hoffelner W 2007 *J. Nucl. Mater.* **362** 253
[17] Béchade J L, Menut D, Lescoat M L, Sitaud B, Schlutig S, Solari P, Llorens I, Hermange H, de Carlan Y, Ribis J and Toualbi L 2012 *J. Nucl. Mater.* **428** 183
[18] He P, Liu T, Möslang A, Lindau R, Ziegler R, Hoffmann J, Kurinskiy P, Commin L, Vladimirov P, Nikitenko S and Silveir M 2012 *Mater. Chem. Phys.* **136** 990
[19] Liu S, Odette G R and Segre C U 2014 *J. Nucl. Mater.* **445** 50
[20] Menut D, Béchade J L, Cammelli S, Schlutig S, Sitaud B and Solari P L 2015 *J. Mater. Res.* **30** 1392
[21] Cintins A, Anspoks A, Purans J, Kuzmin A, Timoshenko J, Vladimirov P, Gräning T and Hoffmann J 2015 *IOP Conf. Ser.: Mater. Sci. Eng.* **77** 012029
[22] Hirata A, Fujita T, Wen Y R, Schneibel J H, Liu C T and Chen M W 2011 *Nat. Mater.* **10** 922
[23] Yashiro K, Yamaguchi A, Tanaka M, Okuda T, Koga K and Segi T 2012 *Mater. Trans.* **53** 401
[24] Alinger M, Wirth B, Lee H J and Odette G 2007 *J. Nucl. Mater.* **367-370** 153
[25] Hin C, Wirth B D and Neaton J B 2009 *Phys. Rev. B* **80** 134118
[26] Kuzmin A and Evarestov R A 2009 *J. Phys.: Condens. Matter* **21** 055401
[27] Bonnet M, Delapalme A and Fuess H 1975 *Acta Cryst. A* **31** 264
[28] Carlson O 1990 *Bull. Alloy Phase Diagrams* **11** 61
[29] Faucher M and Pannetier J 1980 *Acta Cryst. B* **36** 3209
[30] Swamy V, Dubrovinskaya N A and Dubrovinsky L S 1999 *J. Mater. Res.* **14** 456
[31] Bose P P, Gupta M K, Mittal R, Rols S, Achary S N, Tyagi A K and Chaplot S L 2011 *Phys. Rev. B* **84** 094301
[32] Álvarez L J, San Miguel M A and Odriozola J A 1999 *Phys. Rev. B* **59** 11303
[33] Belonoshko A B, Gutierrez G, Ahuja R and Johansson B 2001 *Phys. Rev. B* **64** 184103
[34] Lau K C and Dunlap B I 2011 *J. Phys.: Condens. Matter* **23** 035401
[35] Timoshenko J, Kuzmin A and Purans J 2014 *J. Phys.: Condens. Matter* **26** 055401
[36] Timoshenko J, Kuzmin A and Purans J 2012 *Comput. Phys. Commun.* **183** 1237

[37] Kalinko A, Evarestov R A, Kuzmin A and Purans J 2009 *J. Phys.: Conf. Ser.* **190** 012080
[38] Timoshenko J, Kuzmin A and Purans J 2013 *J. Phys.: Conf. Ser.* **430** 012012
[39] Kuzmin A, Efimov V, Efimova E, Sikolenko V, Pascarelli S and Troyanchuk I 2011 *Solid State Ionics* **188** 21
[40] Timoshenko J, Kuzmin A and Purans J 2011 *Centr. Eur. J. Phys.* **9** 710
[41] Anspoks A, Kalinko A, Kalendarev R and Kuzmin A 2012 *Phys. Rev. B* **86** 174114
[42] Timoshenko J, Anspoks A, Kalinko A and Kuzmin A 2014 *Phys. Status Solidi C* **11** 1493
[43] Timoshenko J, Anspoks A, Kalinko A and Kuzmin A 2014 *Acta Mater.* **79** 194
[44] Kalinko A and Kuzmin A 2013 *J. Phys.: Conf. Ser.* **430** 012075
[45] Timoshenko J, Anspoks A, Kalinko A and Kuzmin A 2014 *Phys. Scripta* **89** 044006
[46] Timoshenko J, Anspoks A, Kalinko A and Kuzmin A 2015 *Phys. Status Solidi A* **212** 265
[47] Di Cicco A, Aquilanti G, Minicucci M, Principi E, Novello N, Cognigni A and Olivi L 2009 *J. Phys.: Conf. Ser.* **190** 012043
[48] Kuzmin A 1995 *Physica B* **208-209** 175
[49] Ankudinov A L, Ravel B, Rehr J J and Conradson S D 1998 *Phys. Rev. B* **58** 7565
[50] Gale J D 1996 *Phil. Mag. B* **73** 3
[51] Gale J D and Rohl A L 2003 *Mol. Simul.* **29** 291
[52] Hoover W G 1985 *Phys. Rev. A* **31** 1695
[53] Hockney R W 1970 *Methods Comput. Phys.* **9** 136
[54] Rehr J J and Albers R C 2000 *Rev. Mod. Phys.* **72** 621
[55] Palko J W, Kriven W M, Sinogeikin S V, Bass J D and Sayir A 2001 *J. Appl. Phys.* **89** 7791
[56] McGreevy R L and Pusztai L 1988 *Mol. Simul.* **1** 359
[57] Muñoz M, Argoul P and Farges F 2003 *Am. Mineral.* **88** 694
[58] Funke H, Scheinost A C and Chukalina M 2005 *Phys. Rev. B* **71** 094110
[59] Timoshenko J and Kuzmin A 2009 *Comp. Phys. Commun.* **180** 920
[60] Sevillano E, Meuth H and Rehr J J 1979 *Phys. Rev. B* **20** 4908
[61] Repelin Y, Proust C, Husson E and Beny J M 1995 *J. Sol. State Chem.* **118** 163
[62] Ubaldini A and Carnasciali M M 2008 *J. Alloy Compd.* **454** 374
[63] Booth C H, Bridges F, Bauer E D, Li G G, Boyce J B, Claeson T, Chu C W and Xiong Q 1995 *Phys. Rev. B* **52** R15745
[64] Sapelkin A V and Bayliss S C 2002 *Phys. Rev. B* **65** 172104
[65] Jeong I K, Heffner R H, Graf M J and Bilinge S J L 2003 *Phys. Rev. B* **67** 104301